



Investigation to Understand the Co Ions Inclusion in Ba₃SnO Antiperovskites Structure

Naveed Jafar¹, G. Murtaza^{1*}, Ghazanfar Nazir^{2*}, Adeela Rehman³

¹ Centre for Advanced Studies in Physics, GC University, Lahore

² Department of Nanotechnology and Advanced Materials Engineering, Sejong University, Seoul 05006, Republic of Korea

³ Department of Chemistry, Inha University, 100 Inharo, Incheon 22212, South Korea

ARTICLE INFO

ABSTRACT

Article History:

Received: September 14, 2021

Revised: November 12, 2021

Accepted: December 29, 2021

Available Online: December 31, 2021

Keywords:

Ba₃SnO

Antiperovskites structure

SRIM

XRD

FTIR

SEM

EDX

The current research focuses on the fabrication and characterization of barium tin oxide antiperovskite oxide Ba₃SnO. BaO and Sn₂O were used as precursors to synthesise the Ba₃SnO by using solid state ceramic method. Co ion has been implanted using Pelletron Accelerator with different doses 10¹³, 5×10¹³, 10¹⁴ ions/cm². The study includes the investigations of penetration depth range of Co ions in the target material, structural, surface morphology, verification of elemental composition, and band gap energy by using the characterization techniques SRIM, XRD, SEM, EDX, FTIR, and UV-Vis spectroscopy respectively. Phase identification of desired material assures by XRD. SEM results showed that the rough and sharp rod shape varies into a very smooth and fine granular shape by ion implantation. EDX plots confirm the existence of basic elements like Ba, Sn, Co and O. The FTIR identify the unknown material and components which confirmed the formation of B₃SnO and incorporation of Co ions. UV-Vis spectroscopy results revealed that increasing the implanted ion dose causes a slight increase in band gap energy from 2.61 to 2.88 of this material. The obtained results allow us to conclude that the prepared sample contains a fine structure with no impurity. Therefore, we can say that this process is ideal for obtaining fine structured Ba₃SnO.

OPEN ACCESS

© 2021 The Authors, Published by iRASD. This is an Open Access article under the Creative Commons Attribution Non-Commercial 4.0

*Corresponding Authors' Email: gmrai@gcu.edu.pk, gnazir@sejong.ac.kr

1. Introduction

Generally, the perovskites are symbolized by the formula ABX₃. If the position of A and X are exchanged, then the new resultant class of material is formed which is called antiperovskite which exhibits cubic or pseudo-cubic structure (Oudah et al., 2016). Then the general formula for antiperovskite is X₃BA, where 'B' and 'A' are two anions of different sizes and 'X' is a cation. In antiperovskite oxide the atom 'B' may be Si, Ge, Sn and Pb, 'A' is oxygen and 'X' may be an element of group IIA such as Ba, Sr, and Ca. Such as perovskite oxides, the antiperovskite oxides also have many physical properties such as superconductivity, electrolytic, electrostriction, piezoelectric, thermoelectric properties, magnetic and optical properties. Antiperovskite oxides have many technological uses like quantum computing, flat panel display, biosensors spintronic devices as well as magneto-resistive devices (Arakawa, Kurachi, & Shiokawa, 1985; Bokov & Ye, 2006; Israel, Calderón, & Mathur, 2007; Kim, Qi, Dahlberg, & Li, 2010; Mathur et al., 1997). Both materials of perovskite oxides and anti-perovskite oxides may be alleviated in other structures such as hexagonal orthorhombic structures. In previous study, scientists have extensively explored the innovative characteristics of anti-perovskites. The anti-perovskites have attained vast desirability to be investigated for the numerous industrial utilities due to

their wide band gap range. The anti-perovskites which have small band gap are potential applicants for numerous optical devices. The anti-perovskites can be appear as non-metals, semiconductors, metals as well as superconductors therefore they have interesting material behaviors (Bilal, Jalali-Asadabadi, Ahmad, & Ahmad, 2015).

Antiperovskite oxides changed their properties by varying the temperature and pressure. In 2010, Hichour et.al (Hichour et al., 2010) explored the $ANSr_3$ (A= As, Sb and Bi) antiperovskite pressure-dependent properties and perceived narrow direct bandgap proposed appropriate optical applications. Some experiments revealed that, Sr_3PbO , Ca_3PbO as well as Ba_3PbO are strong nominees for topological crystalline insulators (Hsieh, Liu, & Fu, 2014; Samal, Nakamura, & Takagi, 2016) and thermoelectric applications (Okamoto, Sakamaki, & Takenaka, 2016). The significant values of this atom configuration were that the 'B' atom in X_3BA antiperovskite attains a negative charge state (e.g., B^{4-}), the also strong overlap of 'p' states of 'B' and 'd' states of 'X' atoms (Batool, Alay-e-Abbas, & Amin, 2017). It is reported that the lattice constant of the cubic structure increases as cation changes from Ca to Ba and it may be increased by increasing the concentration of doped ions (Hassan, Arshad, & Mahmood, 2017). The crystal structure of antiperovskite Ba_3SnO is described as 'Ba' is a cation and 'Sn' as well as 'O' are the anions. In the cubic structure of antiperovskite, 'O' atoms are placed at the corner of the cube, whereas 'Sn' occupied octahedral site and the 'Ba' are placed on the faces of the cube.

This study is an exploration of the properties of novel antiperovskite material i.e. Ba_3SnO . Synthesize and characterization of antiperovskite oxide Ba_3SnO and understanding the inclusion of Co ions in barium tin oxide was the main purpose of this research work. We also analyzed the effect of Co ions implantation in Ba_3SnO . The Synthesis of Ba_3SnO had to be approached from an adequate route as it has not been synthesized before.

2. Experimental Procedure

The materials were selected on the basis of properties, cost and thier suitability. BaO and SnO_2 with desired molecular weight by stoichiometric calculations were used for the preparation of Ba_3SnO . The solid state method was used in this work to prepare Ba_3SnO ; as at room temperature the solid materials do not recombine and react. Therefore, initially materials are heated at higher temperatures to complete the reaction properly (Callister Jr & Rethwisch, 2020). Both precursors BaO and SnO_2 were ground for 2 hours in a mortar pestle and then calcinated the mixture at $900^\circ C$ for 6 hours in the furnace. After calcination, the sample was again ground for 30 min. By using a hydraulic press machine, the desired pellets were formed of 1.5 g at 3000 psi. The whole synthesis process was done under consideration of a given equation:



Fine Ba_3SnO was obtained after sintering the pellets at $600^\circ C$ for 2 hours in the furnace. Finally, the Co ions are implanted on the host material Ba_3SnO by Pelletron Accelerator with different doses 10^{13} , 5×10^{13} , 10^{14} ions/cm². Phase identification was done by using an X-ray diffractometer (XRD).

3. Results and Discussions

3.1. SRIM Analysis

The concept of effective charge was used for establishing the charge state of an ion inside a target material. When sample is exposed to ion a damage occured inside the material which is observed by SRIM. In this project, the penetration of cobalt is observed on the target sample of Ba_3SnO , which is irradiated with various implantation fluence. Figure 1 shows the penetration shape of Co with an energy of 500 keV inside the prepared materials. The penetration depth range of Co is about 1 μm .

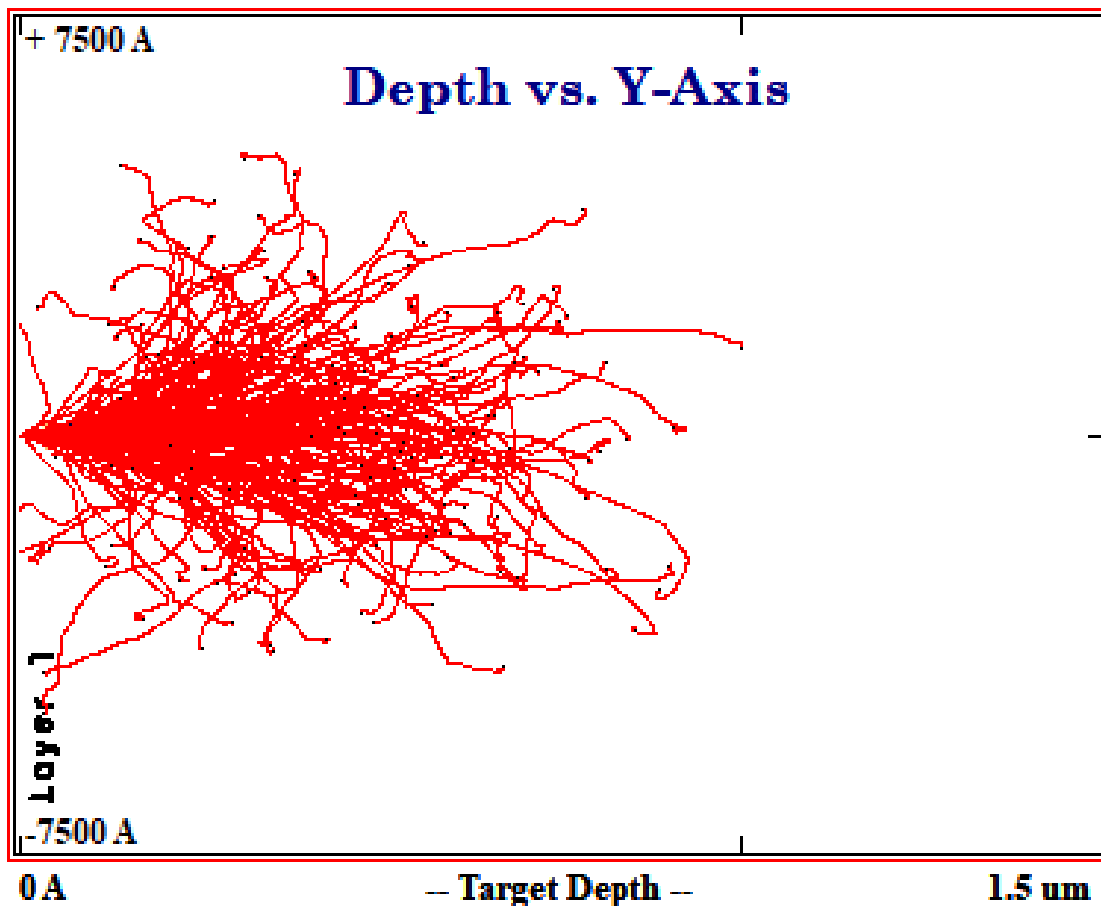


Figure 1: Depth and range of implanted Co ions in Ba₃SnO

3.2. Structural Analysis

X-ray diffraction (XRD) patterns of all the samples are shown in figure 2. XRD result of Ba₃SnO in figure 2(a), the pure untreated sample that represents the existence of an higher intensive peak at angle 31.6° with plane of (111). This is matched with the reported XRD card (JCPDS card no 01-083-1868). The XRD patterns represents the crystalline phase formation of Ba₃SnO and there is no extra peak either due to SnO₂ or any other contamination. The diffraction peaks appear at angles (2θ) of 25.29°, 45.08°, 47.68°, 55.52°, 64.83°, 69.04° and 72.60°, which assigned planes of the crystal lattice of hkl 110, 200, 220, 311, 321, 320 and 411, respectively. The sample is exposed to Co ions having the dose of 1×10^{13} ions/cm² (see figure 2(b)). It is noted that the maximum peak at 31.6° becomes sharper that showing an increase in intensity. It confirms that the crystallinity and quality of the material can enhanced with ion implantation at low influence. The peak appears at angle of 44° denotes Co ions with the plane 111*.

The crystallite size is equal to 37 nm and lattice constant is equal to 4.91Å. Volume of the cell is equal to 118.38 Å³ (see table 1). Enhancement in crystallinity may be due to the electronic excitations or ionization energy (electronic energy loss). When fast moving ion enter inside a solid it loss some of their energy during an elastic collisions between ion and atom of the solid (Agarwal et al., 2006). Table 1 shows that the crystallite size varies from 29 to 37 nm which verify the results that the crystallinity of the material improves after Co ion implantation.

Similarly, in figure 2(c) because of high dose ions of value 5×10^{13} some additional peaks are also appeared. The peak appears at angle of 44° may be due to Co ions, which is evidence for the implanted Co ions. The lattice constant increases from 4.88 to 5.15 Å due to Co ions. The peak appears at angle of 24.6° shows the secondary phase due to BaO that is matched with the Card (JCPDS # 00-001-0746). The increase of lattice constant may be due to the lattice distortion caused by Co ions while the secondary phase caused due to the short time of calcination. The volume of the unit cell is 143.82 Å³ that is changed from the base sample. At higher dose of 5×10^{13} ions/cm² the crystallite size of is found to be 31.5 nm (see table 1) that is smaller than the crystallite size of dose in order of 10^{13} ions/cm². It

signifies that the crystallinity decreases, and density of grains increases (Li & Bergman, 2009; Varadhaseshan, Meenakshi Sundar, & Prema, 2014). Table 1 ensures the presence of Co ions because the lattice increases from 4.88 to 5.15Å.

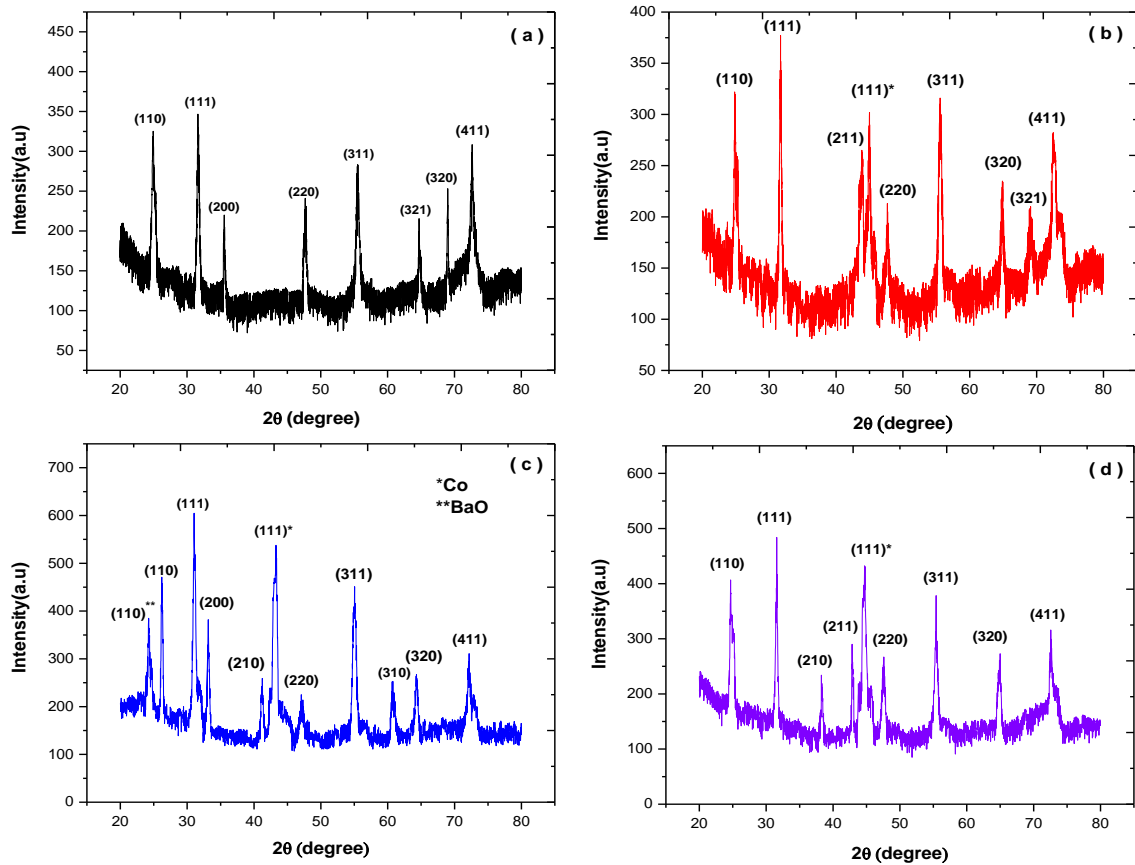


Figure 3 (a, b, c, d): XRD graphs of the pure and doped samples

Similarly, in figure 2(c) because of high dose ions of value 5×10^{13} some additional peaks are also appeared. The peak appears at angle of 44° may be due to Co ions, which is evidence for the implanted Co ions. The lattice constant increases from 4.88 to 5.15 Å due to Co ions. The peak appears at angle of 24.6° shows the secondary phase due to BaO that is matched with the Card (JCPDS # 00-001-0746). The increase of lattice constant may be due to the lattice distortion caused by Co ions while the secondary phase caused due to the short time of calcination. The volume of the unit cell is 143.82 \AA^3 that is changed from the base sample. At higher dose of 5×10^{13} ions/cm² the crystallite size of is found to be 31.5 nm (see table 1) that is smaller than the crystallite size of dose in order of 10^{13} ions/cm². It signifies that the crystallinity decreases, and density of grains increases (Li & Bergman, 2009; Varadhaseshan et al., 2014). Table 1 ensures the presence of Co ions because the lattice increases from 4.88 to 5.15Å.

Similarly, in figure 2(d) the intensity of the main crystalline peak at (111) is decreased reduction ensured by an increment in FWHM which implies that the crystallite size reduces. The crystallite size for 5×10^{13} ions/cm² dose is 31.5 nm but for the dose of 1×10^{14} ions/cm² crystallite size is 30 nm. The lattice constant increases from 4.88 Å to 5.23 Å (Agarwal et al., 2006).

Table 1
Calculated lattice parameters of pure and Co doped samples

Samples	Lattice constants (Å) a=b=c	Cell volume (Å ³) V	Crystallite size (nm) D
Pure	4.88	116.50	29
10^{13}	4.9	118.38	37
5×10^{13}	5.15	143.82	31.5
10^{14}	5.23	136.27	30

3.3. Surface Analysis

SEM micrographs analysis in figure 3(a, b, c, d) displays the surface morphology of pure as well as doped Ba_3SnO samples. Since, melting point of magnetic ceramic material is very high, therefore for various materials at higher temperature O loss occurs before melting. A polycrystalline structure is formed by sintering. The prepared sample is calcined at temperature of 900°C for 8 hours. Polycrystalline is formed from the bonded of tiny crystals together. Figure 3(a) for the pure sample of Ba_3SnO displays rod formation as well as a sharp and raw surface. The stout bright spots are also observed in figure 3(a, b, c, d) which shows pores inside the material (Mujahid, Sarfraz, & Amin, 2015).

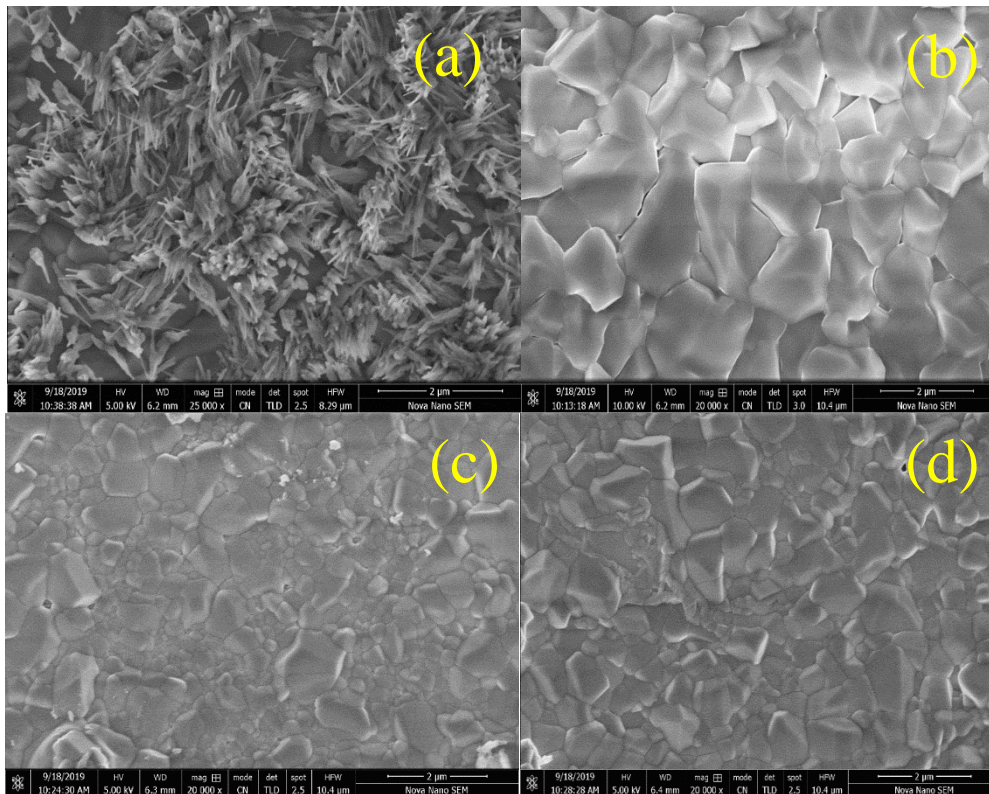


Figure 3(a, b, c, d): SEM micrographs of untreated and treated samples (a) untreated (b) 1×10^{13} (c) 5×10^{13} (d) 1×10^{14}

Figure 3(b) displays that the grain growth occurs for Co ion implanted of the dose 10^{13} ions/cm². The calculated average grain size is $1.3 \mu\text{m}$ increases from $0.76 \mu\text{m}$ of pure sample and these results match with the XRD results. The morphology of the Ba_3SnO changes from rough surface to a smaller dense surface. This is due to the energetic cobalt ions, when bombarded on material then it transfer their energy to Ba_3SnO which lead to the formation required material (Murtaza et al., 2011).

Similarly, both dopants with the dose of 5×10^{13} ions/cm² as well as 10^{14} ions/cm² ions reduces the grain size to produce microstructures. In figure 3(c) shows grain size is $0.8 \mu\text{m}$ for dose of 5×10^{13} ions/cm² while figure 3(d) shows grain size is $0.7 \mu\text{m}$ for the dose of 10^{14} ions/cm². Since density of dopant (Co) increases, which caused an increase of the grain boundaries. The increase of grain boundaries caused the decrease in grain size (Park, Jung, Kim, & Park, 2008).

3.4. EDX Analysis

EDX studies were performed to confirm an elemental composition of the material. As the basic elements are Ba, Sn and O. Figure 4(a, b, c, d) shows EDX spectra which indicate the peaks which ensure the existence of Ba, O and Sn in Ba_3SnO sample. There is an extra peak of S which may be due to contamination or come from the sample holder. In figure 4(b, c, d) there is slight difference in peak's intensity of Co ion because ion dose increase from the value of 1×10^{13} , 5×10^{13} and 1×10^{14} ions/cm² (Tabari, Tavakkoli, Zargaran, & Beiknejad, 2012).

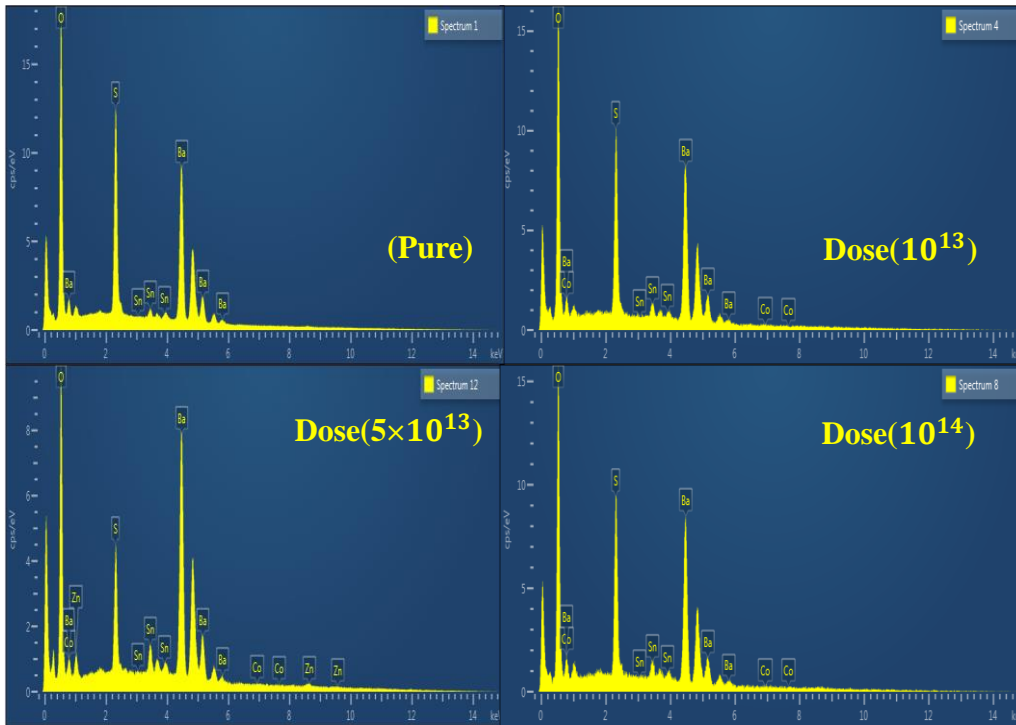


Figure 4(a, b, c, d): EDX graphs of pure and doped Ba_3SnO

3.5. FTIR Analysis

It has been shown that FTIR spectroscopy is proper and suitable device for understanding the functional group of any compound. FTIR analysis confirmed the bond formation of barium tin oxide and the incorporation of 'Co' ions in the crystal lattice. Figure 5 show the FTIR spectra of the calcined material at temperature of 900°C for 8 hours. The broad peak observed at wavenumber of 1429 cm^{-1} , is due to stretching vibration of Ba-O bond (Kumari, Suresh, & Rao, 2013; Lu & Schmidt, 2007; Murtaza et al., 2011). The peak is at wavenumber of 3311.77 cm^{-1} is due to the stretching vibration of O-H bond. The peaks at wavenumber of 850.62 cm^{-1} is due to absorption of CO_2 and stretching vibration of CO_3^{2-} (Durán, Gutierrez, Tartaj, Bañares, & Moure, 2002; Lu & Schmidt, 2008). Similarly, the peaks at wavenumbers of 640.36 cm^{-1} and the 1721.36 cm^{-1} are due to the stretching vibration of Sn-O and Co-O, respectively (Bazeera & Amrin, 2017; Varadhaseshan et al., 2014). All observed peaks are agreed with the reported data in the literature.

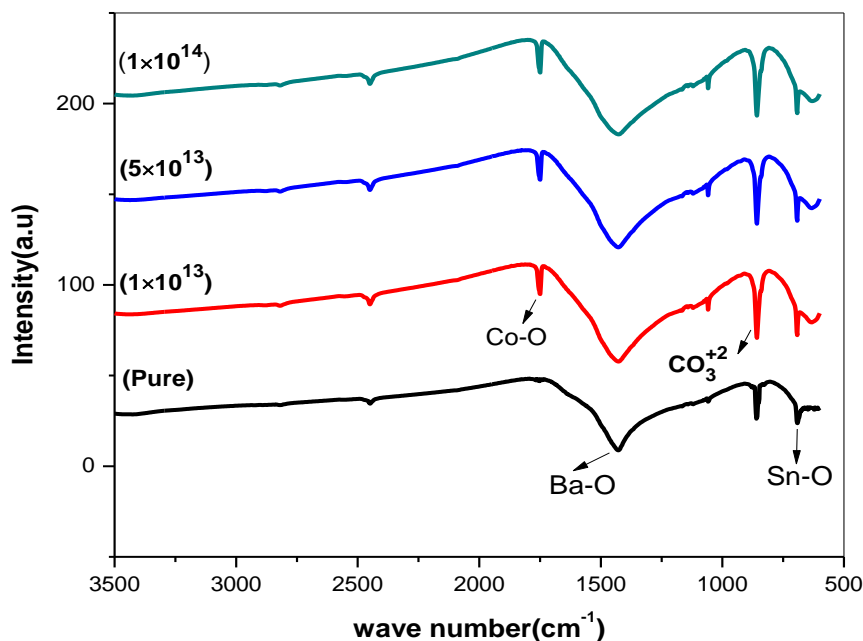


Figure 5: FTIR spectra for pure and doped Ba_3SnO

3.6. Bandgap Analysis

The optical characterization of pure and cobalt doped material was studied by UV-Vis spectroscopy. It offers beneficial information about the bandgap study of semiconductor pure barium tin oxide and the effect of Co ions implantation doping on the bandgap of the host material. A semiconductor is characterized by its electronic band structure. The energy difference between the highest occupied molecular orbital (HOMO) and the lowest unoccupied molecular orbital (LUMO) is termed as band gap energy (E_g). The optical absorption study of the irradiated and pristine was carried out and the bandgap of the films have been calculated using Tauc's plot by plotting $(\alpha h\nu)^2$ versus $h\nu$ and extrapolating the linear portion of the absorption edge to find the intercept with energy axis. The energy of on photon is calculated by the relation $E = hc / \lambda$. In the high energy absorption region dependence on photon energy is expressed by Tauc's equation. On the basis of Tauc relation, the absorption coefficient " α " for direct bandgap material is given by:

$$\alpha(h\nu) = B(h\nu - E_g)^m \quad (2)$$

From figure 6 of Tauc's plots, it is clear that the bandgap of Ba_3SnO slightly varied from 2.61 to 2.88. The presence of Co ions causes the change in the bandgap of barium tin oxide. Tauc plots reveal that absorption is in the range of 200 to 800 nm. The reason for the increase in the energy bandgap in the visible region of exposed materials is because of the interstitial location formed by Co ions. Since, Co is metal, which provides extra electrons so the existence of Co ions at the interstitial location causes the charge transition between the narrow band of the localized Co state and conduction state of the host which cause in increase in band gap (Deepa et al., 2011). The increase of bandgap may because of dopant concentration, surface effects, lattice strain and quantum confinement effects (Chen, Lou, Samia, & Burda, 2003; Nandan, Venugopal, Amirthapandian, Panigrahi, & Thangadurai, 2013; Smith, Mohs, & Nie, 2009).

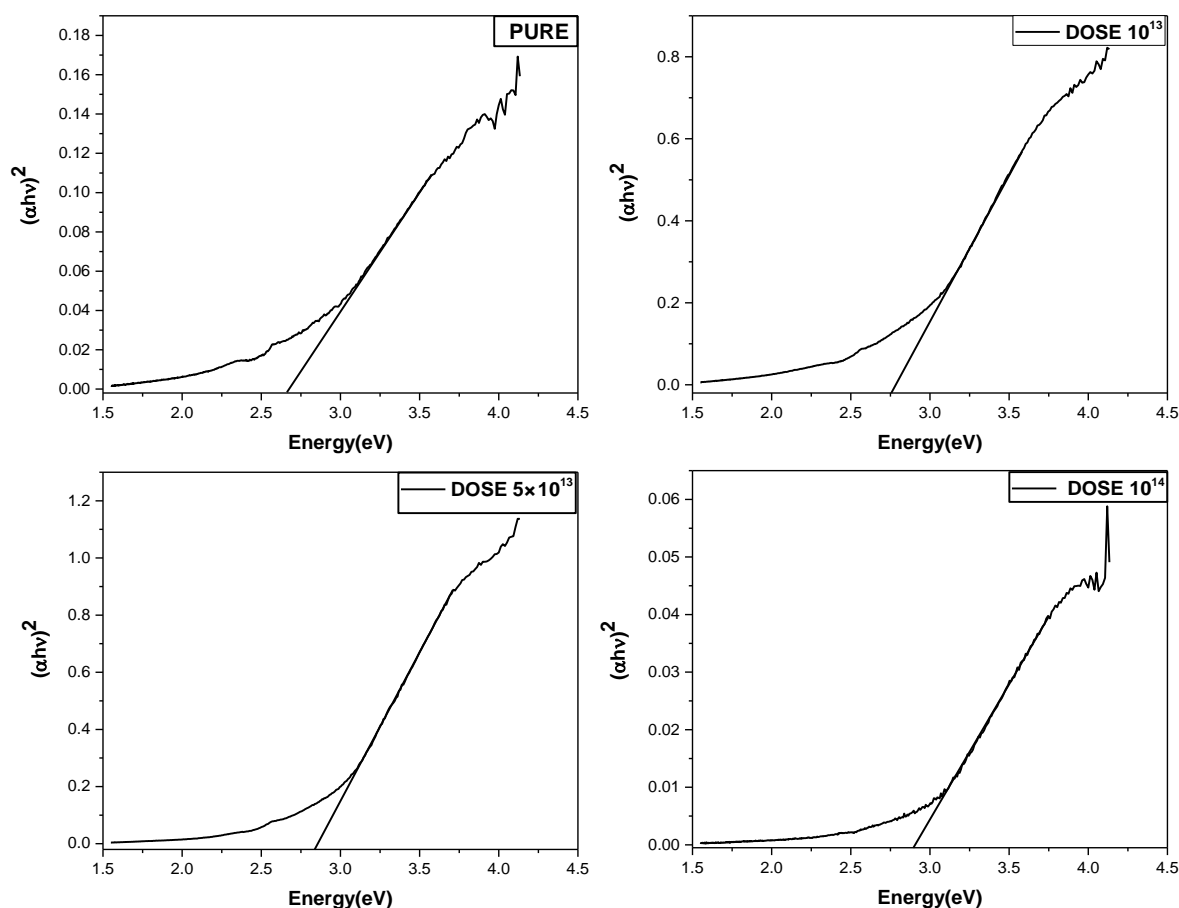


Figure 6: Tauc plots results for pure Ba_3SnO and doped Ba_3SnO

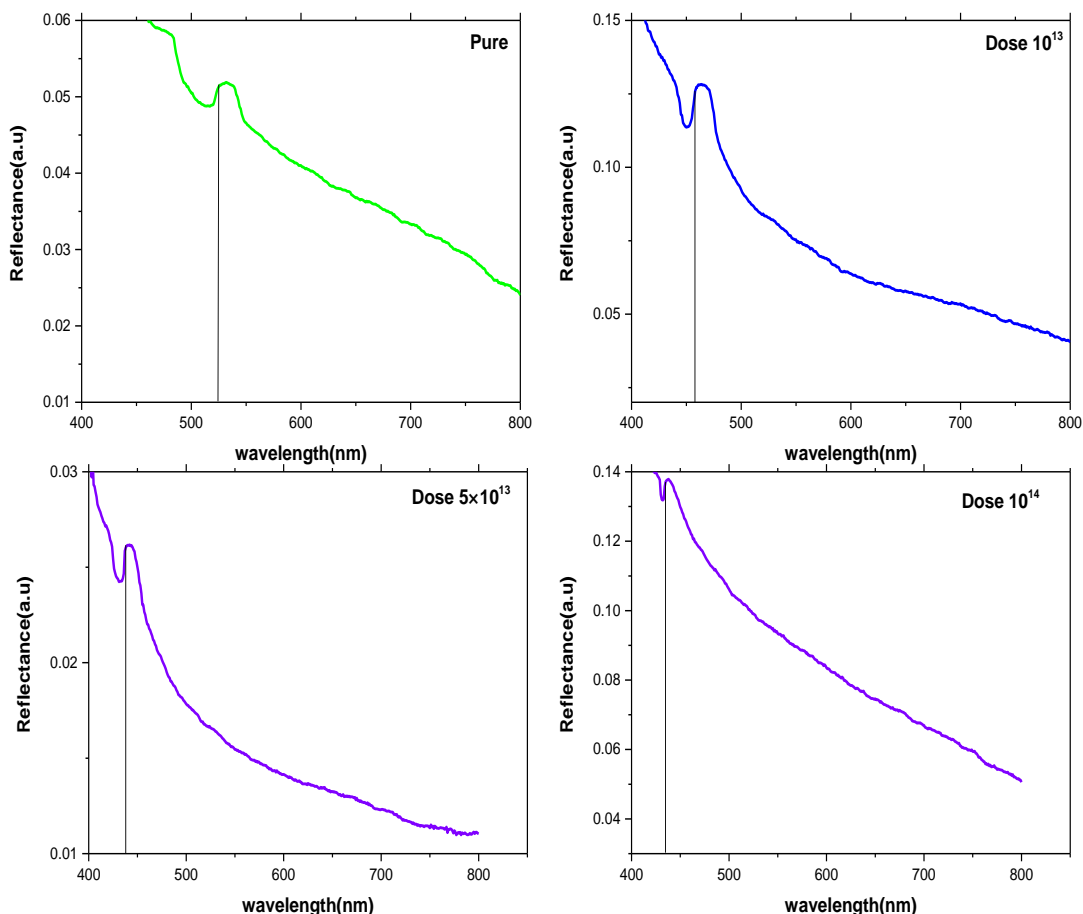


Figure 7: Reflectance graphs for pure Ba_3SnO and doped Ba_3SnO

Reflectance spectrum as shown in figure 7 for pure sample indicates the maximum reflectance of light heavily at 535 nm a green emission and has energy 2.32 eV. Similarly, the figure for doped samples shows when the material is irradiated by Co ions 10^{13} ions/cm² a blue emission takes place at 464 nm and has an energy of 2.67. Similarly, it is noted that decreasing values of wavelengths causes the increase in values of energy from 2.73 to 2.88 eV by variance in a dose of implanted Co ions 5×10^{13} ions/cm² and 1×10^{14} ions/cm² correspondingly causes the violet emission which indicated that the sample corresponds the visible region. It is clear from the graph that there is no significant variation in band edge after the irradiation, but the absorption lies in the visible region. This implies that the basic crystal structure is not changed.

4. Conclusion

In this work, antiperovskite oxide Ba_3SnO was successfully synthesized using solid state method and subsequently, Co ions with different ions fluence were embedded into Ba_3SnO structure using the ion implantation route. XRD results confirm the cubic structure of barium tin oxide. Results also reveal that the lattice parameters increase from 4.88 Å to 5.2 Å after Co ion implantation that becomes more prominent at the highest dose 10^{14} ions/cm². The crystallinity of material is enhanced for low values 10^{13} ions/cm² and decreases by increasing the fluence up to dose 10^{14} ions/cm². The rods shape formation of the undoped sample changes into a fine granular shape by increasing the fluence from 10^{13} to 10^{14} ions/cm² of Co ions, which has been confirmed by FE-SEM. Surface morphology also shows the grain size reduces from 1.33 to 0.7 μm by increasing the higher dose 10^{14} ions/cm² match with the XRD results. FTIR study confirms the formation of barium tin oxide by showing that the functional groups are present in all the samples and ensures the presence of Co ions. UV-vis spectrometer was used to analyse the energy band gap of Ba_3SnO . The results exhibit the increases of energy bandgap from 2.61 to 2.88 eV by

increasing the fluence of ions from 10^{13} to 10^{14} ions/cm². From all the investigations, the conclusion drawn that the inclusion of Co is fruitful to alter the optical properties of Ba₃SnO.

References

- Agarwal, D. C., Kumar, A., Khan, S. A., Kabiraj, D., Singh, F., Tripathi, A., . . . Avasthi, D. K. (2006). SHI induced modification of ZnO thin film: Optical and structural studies. *Nuclear Instruments and Methods in Physics Research Section B: Beam Interactions with Materials and Atoms*, 244(1), 136-140. doi:<https://doi.org/10.1016/j.nimb.2005.11.077>
- Arakawa, T., Kurachi, H., & Shiokawa, J. (1985). Physicochemical properties of rare earth perovskite oxides used as gas sensor material. *Journal of materials science*, 20(4), 1207-1210. doi:10.1007/BF01026315
- Batool, J., Alay-e-Abbas, S. M., & Amin, N. (2017). Thermodynamic, electronic, and magnetic properties of intrinsic vacancy defects in antiperovskite Ca₃SnO. *Journal of Applied Physics*, 123(16), 161516. doi:10.1063/1.4994998
- Bazeera, A. Z., & Amrin, M. I. (2017). Synthesis and characterization of barium oxide nanoparticles. *IOSR J. Appl. Phys*, 1, 76-80.
- Bilal, M., Jalali-Asadabadi, S., Ahmad, R., & Ahmad, I. (2015). Electronic Properties of Antiperovskite Materials from State-of-the-Art Density Functional Theory. *Journal of Chemistry*, 2015, 495131. doi:10.1155/2015/495131
- Bokov, A., & Ye, Z. (2006). 2006JMatS. 41.31 B. vol. 41. *J. Mater. Sci*, 31.
- Callister Jr, W. D., & Rethwisch, D. G. (2020). *Callister's materials science and engineering*: John Wiley & Sons.
- Chen, X., Lou, Y., Samia, A. C., & Burda, C. (2003). Coherency Strain Effects on the Optical Response of Core/Shell Heteronanostructures. *Nano Letters*, 3(6), 799-803. doi:10.1021/nl034243b
- Deepa, A. S., Vidya, S., Manu, P. C., Solomon, S., John, A., & Thomas, J. K. (2011). Structural and optical characterization of BaSnO₃ nanopowder synthesized through a novel combustion technique. *Journal of Alloys and Compounds*, 509(5), 1830-1835. doi:<https://doi.org/10.1016/j.jallcom.2010.10.056>
- Durán, P., Gutierrez, D., Tartaj, J., Bañares, M. A., & Moure, C. (2002). On the formation of an oxycarbonate intermediate phase in the synthesis of BaTiO₃ from (Ba,Ti)-polymeric organic precursors. *Journal of the European Ceramic Society*, 22(6), 797-807. doi:[https://doi.org/10.1016/S0955-2219\(01\)00392-2](https://doi.org/10.1016/S0955-2219(01)00392-2)
- Hassan, M., Arshad, I., & Mahmood, Q. (2017). Computational study of electronic, optical and thermoelectric properties of X₃PbO (X = Ca, Sr, Ba) anti-perovskites. *Semiconductor Science and Technology*, 32(11), 115002. doi:10.1088/1361-6641/aa8afe
- Hichour, M., Khenata, R., Rached, D., Hachemaoui, M., Bouhemadou, A., Reshak, A. H., & Semari, F. (2010). FP-APW+lo study of the elastic, electronic and optical properties for the cubic antiperovskite ANSr₃ (A=As, Sb and Bi) under pressure effect. *Physica B: Condensed Matter*, 405(7), 1894-1900. doi:<https://doi.org/10.1016/j.physb.2010.01.069>
- Hsieh, T. H., Liu, J., & Fu, L. (2014). Topological crystalline insulators and Dirac octets in antiperovskites. *Physical Review B*, 90(8), 081112. doi:10.1103/PhysRevB.90.081112
- Israel, C., Calderón, M. J., & Mathur, N. D. (2007). The current spin on manganites. *Materials Today*, 10(10), 24-32. doi:[https://doi.org/10.1016/S1369-7021\(07\)70242-0](https://doi.org/10.1016/S1369-7021(07)70242-0)
- Kim, C. H., Qi, G., Dahlberg, K., & Li, W. (2010). Strontium-doped perovskites rival platinum catalysts for treating NO_x in simulated diesel exhaust. *Science*, 327(5973), 1624-1627.
- Kumari, U. S., Suresh, P., & Rao, A. P. (2013). Solid-state metathetic synthesis of phase pure BaSnO₃ and BaZrO₃. *International Research Journal of Pure and Applied Chemistry*, 3(4), 347.
- Li, S., & Bergman, B. (2009). Doping effect on secondary phases, microstructure and electrical conductivities of LaGaO₃ based perovskites. *Journal of the European Ceramic Society*, 29(6), 1139-1146. doi:<https://doi.org/10.1016/j.jeurceramsoc.2008.08.017>

- Lu, W., & Schmidt, H. (2007). Synthesis of nanosized BaSnO₃ powders from metal isopropoxides. *Journal of Sol-Gel Science and Technology*, 42(1), 55-64. doi:10.1007/s10971-006-1508-4
- Lu, W., & Schmidt, H. (2008). Lyothermal synthesis of nanocrystalline BaSnO₃ powders. *Ceramics International*, 34(3), 645-649. doi:<https://doi.org/10.1016/j.ceramint.2007.01.002>
- Mathur, N. D., Burnell, G., Isaac, S., Jackson, T., Teo, B.-S., MacManus-Driscoll, J., . . . Blamire, M. (1997). Large low-field magnetoresistance in La_{0.7}Ca_{0.3}MnO₃ induced by artificial grain boundaries. *Nature*, 387(6630), 266-268.
- Mujahid, M., Sarfraz, S., & Amin, S. (2015). On the formation of hydroxyapatite nano crystals prepared using cationic surfactant. *Materials Research*, 18, 468-472.
- Murtaza, G., Hussain, S. S., Rehman, N. U., Naseer, S., Shafiq, M., & Zakauallah, M. (2011). Carburizing of zirconium using a low energy Mather type plasma focus. *Surface and Coatings Technology*, 205(8), 3012-3019. doi:<https://doi.org/10.1016/j.surfcoat.2010.11.015>
- Nandan, B., Venugopal, B., Amirthapandian, S., Panigrahi, B. K., & Thangadurai, P. (2013). Effect of Pd ion doping in the band gap of SnO₂ nanoparticles: structural and optical studies. *Journal of nanoparticle research*, 15(10), 1999. doi:10.1007/s11051-013-1999-1
- Okamoto, Y., Sakamaki, A., & Takenaka, K. (2016). Thermoelectric properties of antiperovskite calcium oxides Ca₃PbO and Ca₃SnO. *Journal of Applied Physics*, 119(20), 205106.
- Oudah, M., Ikeda, A., Hausmann, J. N., Yonezawa, S., Fukumoto, T., Kobayashi, S., . . . Maeno, Y. (2016). Superconductivity in the antiperovskite Dirac-metal oxide Sr_{3-x}SnO. *Nature Communications*, 7(1), 13617. doi:10.1038/ncomms13617
- Park, J. H., Jung, C. H., Kim, D. J., & Park, J. Y. (2008). Effect of H₂ dilution gas on the growth of ZrC during low pressure chemical vapor deposition in the ZrCl₄-CH₄-Ar system. *Surface and Coatings Technology*, 203(1), 87-90. doi:<https://doi.org/10.1016/j.surfcoat.2008.08.004>
- Samal, D., Nakamura, H., & Takagi, H. (2016). Molecular beam epitaxy of three-dimensional Dirac material Sr₃PbO. *APL Materials*, 4(7), 076101.
- Smith, A. M., Mohs, A. M., & Nie, S. (2009). Tuning the optical and electronic properties of colloidal nanocrystals by lattice strain. *Nature Nanotechnology*, 4(1), 56-63. doi:10.1038/nnano.2008.360
- Tabari, T., Tavakkoli, H., Zargaran, P., & Beiknejad, D. (2012). Fabrication of perovskite-type oxide BaPbO₃ nanoparticles and their efficiency in photodegradation of methylene blue : research article. *South African Journal of Chemistry*, 65(1), 239-244. doi:10.10520/EJC127433
- Varadhaseshan, R., Meenakshi Sundar, S., & Prema, C. (2014). On the preparation, structural and magnetic properties of ZnO:Co nanoparticles. *The European Physical Journal - Applied Physics*, 66(1), 10602. doi:10.1051/epjap/2014130316